Langmuir

Article

pubs.acs.org/Langmuir

Design of a Multi-Dopamine-Modified Polymer Ligand Optimally Suited for Interfacing Magnetic Nanoparticles with Biological Systems

Wentao Wang,[†] Xin Ji,[†] Hyon Bin Na,[†] Malak Safi,[†] Alexandra Smith,[‡] Goutam Palui,[†] J. Manuel Perez,[‡] and Hedi Mattoussi*[,†]

[†]Department of Chemistry and Biochemistry, Florida State University, 95 Chieftan Way, Tallahassee, Florida 32306, United States

[‡]Nanoscience Technology Center and Department of Chemistry, University of Central Florida, 12424 Research Parkway, Orlando, Florida 32826, United States

Supporting Information

ABSTRACT: We have designed a set of multifunctional and multicoordinating polymer ligands that are optimally suited for surface functionalizing iron oxide and potentially other magnetic nanoparticles (NPs) and promoting their integration into biological systems. The amphiphilic polymers are prepared by coupling (via nucleophilic addition) several amine-terminated dopamine anchoring groups, poly(ethylene glycol) moieties, and reactive groups onto a poly(isobutylene-*alt*-maleic anhydride) (PIMA) chain. This design greatly benefits from the highly efficient and reagent-free one-step reaction of maleic anhydride groups with amine-containing molecules. The availability of several dopamine groups in the same ligand greatly enhances the ligand affinity, via multiple coordination, to the magnetic NPs, while the hydrophilic and reactive groups promote colloidal stability in buffer media and allow subsequent conjugation with target biomolecules. Iron oxide nanoparticles ligand exchanged with these polymer ligands have a compact hydrodynamic size and exhibit enhanced long-term colloidal stability over the pH range of 4−12 and in the presence of excess electrolytes. Nanoparticles ligated with terminally reactive polymers have been easily coupled to target dyes and tested in live cell imaging with no measurable cytotoxicity. Finally, the resulting hydrophilic nanoparticles exhibit large and size-dependent r_2 relaxivity values.

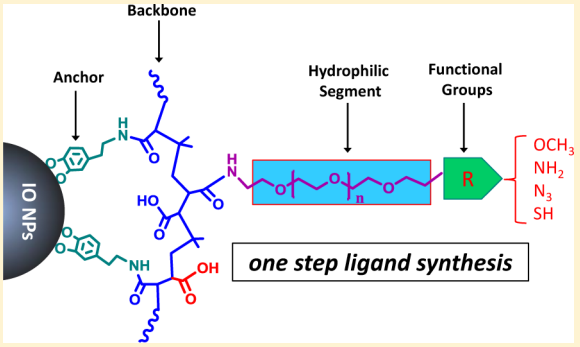

Magnetic nanoparticles such as those made of Fe_3O_4, FePt, Co, or Mn-doped Fe_3O_4 exhibit unique size- and composition-dependent physical properties that are not observed on the molecular scale or shared by their bulk parent materials.[1−7] This has generated a great deal of interest in integrating them into electronic devices and as contrast enhancement agents for magnetic resonance imaging (MRI).[1−4,6,7] Other potential applications in biology include their use as magnetic carriers for drug delivery platforms, biosensors, hyperthermia, and bioseparation.[8−13] Magnetic NPs as contrast-enhancing agents for MR imaging and sensing have attracted considerable attention and much work in the past decade. This has motivated researchers to develop new synthesis schemes to prepare large quantities of high-quality magnetic nanoparticles and to conceive new surface-functionalization strategies for postgrowth manipulation and processing.

An effective integration of magnetic NPs into biology requires the availability of NPs with homogeneous composition, reduced size distribution, high coercivity, and the ability to interface them with biological systems. Thus far, the most successful route to preparing high-quality iron oxide (IO) NPs with controllable size and high crystallinity has relied on the thermal decomposition of metal precursors (such as iron oleate, iron pentacarbonyl, and iron acetylacetonate) in hot surfactant solution.[14−18] However, nanocrystals synthesized via the thermolysis of organometallic precursors are capped with hydrophobic ligands, which make them dispersible only in organic solvents. Therefore, any use in bioinspired investigations requires additional chemical manipulation and postgrowth surface modification to render the magnetic NPs colloidally stable in buffer media and biocompatible.[4,19−22]

Two main strategies have emerged as reliable approaches for interfacing these materials with biological systems. One uses amphiphilic polymers (e.g., copolymers and phospholipids) to encapsulate the as-prepared hydrophobic nanoparticles within micelle-like structures; it relies on the interdigitation (an entropy-driven process) between the hydrophobic segments of the polymers and the native cap. Such a strategy has been employed by several groups to prepare various water-soluble NPs and to couple them to biomolecules.[23−30] Encapsulation

Received: March 21, 2014
Revised: May 7, 2014
Published: May 8, 2014

   dx.doi.org/10.1021/la500974r | *Langmuir* 2014, 30, 6197−6208

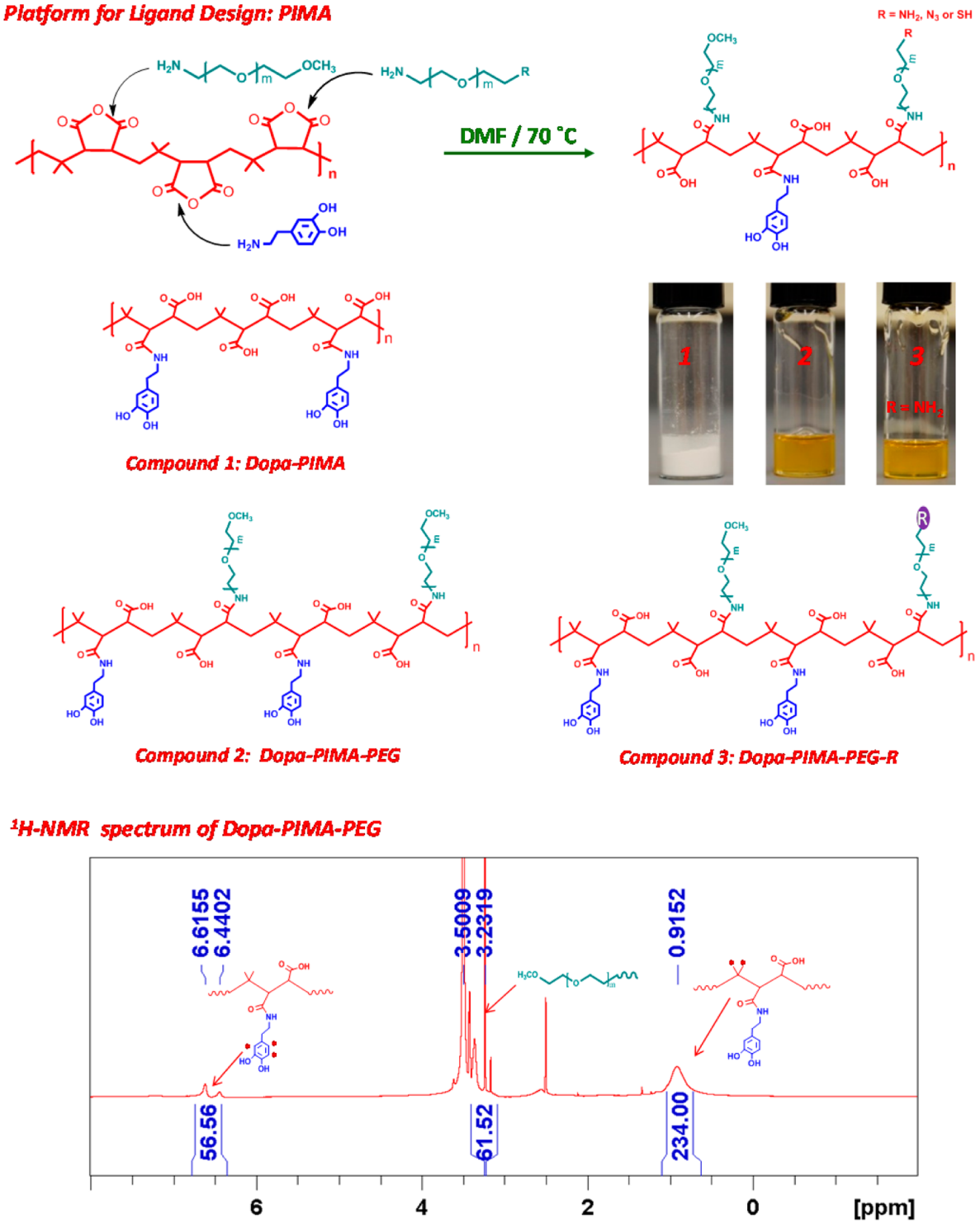

Figure 1. (Top) Schematic representation of the one-step nucleophilic addition applied to the various dopamine-based polymer ligands. (Middle) Structures of three representative ligands reacted with different amine-containing molecules: Dopa-PIMA (compound **1**), Dopa-PIMA-PEG (compound **2**), and Dopa-PIMA-PEG-R (compound **3**). (Bottom) ^{1}H NMR spectrum of Dopa-PIMA-PEG measured in DMSO-d_6. The signatures of multiplet peaks at 6.4–6.7 ppm (from the aromatic proton of catechol), a sharp peak at 3.23 ppm (from the methoxy group of PEG), and a broad peak around 0.9 ppm (from the methyl groups of PIMA) were measured in the NMR spectrum.

preserves the native organic cap, which may be beneficial as this can better preserve the physical properties of the native materials (e.g., optical or magnetic), but tends to significantly increase the hydrodynamic size of the nanoparticles and may yield more than one nanocrystal per micelle.[23,30] This will limit their use in applications requiring small probes. The other strategy relies on removing the hydrophobic shell and replacing it with bifunctional ligands that present anchoring groups and hydrophilic moieties: ligand exchange. These anchors interact with the metal surface via Lewis-base-type coordination. This route should, in principle, provide compact NPs and better colloidal stability under physiological conditions if the ligands

dx.doi.org/10.1021/la500974r | *Langmuir* 2014, 30, 6197–6208

present strong anchoring groups to NP surfaces. For Fe_3O_4 and γ-Fe_2O_3 magnetic nanocrystals, dopamine has been reported to exhibit a specific affinity for the NP surface, a feature attributed to the improved orbital overlap of the five-membered catechol ring and reduced steric effects.[9,31]

Several monodentate dopamine-modified ligands, such as dopamine-PEG-carboxy/amine and zwitterionic dopamine sulfonate, have been used to prepare colloidal dispersions of iron oxide NPs in water media due to the ease of implementation.[32−34] Similarly, ligation with monodentate moieties has been applied to transfer a wide range of inorganic nanocrystals (e.g., metal NPs and quantum dots) to buffer media. However, the binding affinity of such monodentate ligands to the NP surface is weak, and this can result in irreversible ligand desorption from the NP surfaces due to the dynamic nature of coordination interactions. This can negatively affect the NP stability in biological media, in particular at low concentrations. Furthermore, ligands with weak affinity can be easily displaced by biomolecules bearing amine and carboxylic functional groups, which will eventually promote NP aggregation, making this strategy ineffective.[22] Such problems should be overcome by developing multi-coordinating ligands, which improve the NP colloidal stability in biological media by enhancing the ligand affinity for the NP surfaces.[35−40] Our group has previously reported the design of a multi-dopamine-modified ligand consisting of a short poly(acrylic acid) (PAA) backbone laterally appended with a few catechol groups and several poly(ethylene glycol) (PEG) moieties via *N*,*N*′-dicyclohexylcarbodiimide (DCC) and *N*-(3-(dimethylamino)propyl)-*N*′-ethylcarbodiimide (EDC) condensation.[40] The resulting aqueous IO NPs were stable for 1 month under highly acidic/basic conditions and for at least 6 months in DI water. However, the use of the poly(acrylic acid) (PAA) precursor for modification, where the close proximity of the COOH groups along the backbone was combined with the need to use DCC/EDC reagents, produced ligands with lower numbers of metal-coordinating groups (∼6 dopamines per PAA chain); the PAA-based ligands also required thorough postsynthesis purification.

In the present study, we have built on these ideas and designed a new set of amphiphilic polymers as ligands that can promote the dispersion of IO NPs in buffer media with great colloidal stability over a broad range of conditions. The ligands simultaneously present hydrophilic moieties, orthogonally reactive groups, and several anchoring groups. The polymer platform is synthesized using the nucleophilic addition of several amine-presenting anchoring groups (here dopamine) and hydrophilic and reactive moieties onto a poly(isobutylene-*alt*-maleic anhydride) (PIMA) precursor. This ligand design greatly benefits from the high efficiency of the addition reaction since maleic anhydride is highly reactive with any amine-presenting molecule. Furthermore, this reaction can be carried out without the need for additional reagents or excess reactants while allowing the simultaneous coupling of all desired groups in one step.

These polymer ligands have provided a set of compact hydrophilic iron oxide NPs that exhibit excellent colloidal stability over a broad pH range in the presence of excess electrolytes over at least 1 year. Dynamic light scattering measurements confirmed the colloidal stability and relative compactness of the resulting NPs. We also conjugated Cy3 dye to amine-functionalized NPs, yielding a dual-mode optical-MRI platform, which was used for cell imaging with good biodistribution. Viability assays using MTT (3-(4,5-dimethylthiazol-2-yl)-2,5-diphenyltetrazolium bromide) showed that the hydrophilic NPs exhibit no measurable toxicity to live cells. Additional MRI relaxometry experiments showed that these NPs exhibit a size- and concentration-dependent T_2 relaxation effect, with large size-dependent r_2 relaxivity values.

RESULTS AND DISCUSSION

Ligand Design. The polymer ligands developed in this study to promote the transfer of iron oxide nanoparticles from hydrophobic to aqueous media while conferring on them biocompatibility, take advantage of a few unique features of poly(isobutylene-*alt*-maleic anhydride). One of them is the efficiency of the addition reaction between anhydride rings and amine groups. Indeed, maleic anhydride is highly reactive, via nucleophilic addition, with any amine-presenting molecule. This coupling reaction can be carried out in organic media and without the need for additional reagents, which simplifies the purification steps and the ensuing characterization of the prepared materials. Furthermore, the availability of several maleic anhydride rings per polymer chain allows the grafting of multiple lateral groups with distinct chemical functionalities. In particular, it permits a straightforward and controlled insertion of several coordinating groups in the same polymer, which enhances the ligand-to-nanocrystal binding affinity (see Figure 1).[20] It can also allow the introduction of highly biocompatible moieties (e.g., short PEG chains or zwitterion groups) and reactive functional groups (amine, azide, or thiol), which will allow further coupling to target molecules while drastically reducing nonspecific interactions. We should also note that poly(isobutylene-*alt*-maleic anhydride), being a copolymer (where anhydride rings alternate with the dimethylpropane groups) along the chain, presents a few chemical advantages. For example, the presence of dimethyl groups between adjacent anhydride rings reduces steric constraints and enhances their reactivity, allowing high degrees of substitutions during the addition reaction. Thus, larger numbers of anchoring groups and hydrophilic/reactive moieties can be introduced into the amphiphilic ligand. This constitutes a substantial improvement over the oligo-PEG-Dopa ligand design reported in our previous study.[40] Though a smaller-molecular-weight PAA polymer was used in that study, we found that the close proximity of the carboxy groups, combined with the need to use the DCC/EDC condensation reaction to graft dopamines and PEGs onto the PAA backbone, did not allow the insertion of large numbers of anchoring groups; fewer than six dopamine groups per polymer ligands were introduced.[40] In addition, because the DCC/EDC coupling reaction generates rather large quantities of side products (e.g., urea) along with unreacted precursors, additional purification steps were required to isolate the final product. Such constraints are also encountered with other polymer designs for either ligand exchange or encapsulation.[25,40] The present PIMA precursor addresses most of these issues. We should also stress that the present ligand design (and the surface functionalization strategy as a whole) is drastically different from the one relying on encapsulation within an amphiphilic block copolymer described in previous studies, albeit both routes start with similar PIMA precursors.[25−27] Our approach requires the removal of the native cap since the metal chelating groups must interact directly with the nanoparticle surface. We were able to introduce a larger variety of PEG and dopamine moieties into the same polymer ligand. Furthermore, this ligand design

dx.doi.org/10.1021/la500974r | *Langmuir* 2014, 30, 6197−6208

provided Fe_3O_4 NPs with a smaller hydrodynamic size and substantially improved the colloidal stability while allowing surface reactivity (see below). This produces a two-dimensional dense polymer coating layer on the NPs, a result that reflects the strong coordination onto the metal-rich surface and the use of rather small PEG chains.

We started with commercially available PIMA ($M_w \approx 6$ kDa).[26] The maleic anhydride rings were either fully or partially reacted to provide controlled numbers of side groups bound to the backbone via an amide bond; it also frees several carboxylic groups (as many as the number of maleic anhydride rings present), which can provide additional hydrophilic and potential reactive groups in the final compound. We anticipate that for the molecular weight of polymer reported by the manufacturer the average number of monomers per PIMA chain (or index of polymerization) is equal to 39; a mass for the monomer unit of ∼154 g/mol was used. During synthesis, we adjusted the molar amount of each amine-containing moiety with respect to the overall molar amount of monomer units in the precursor polymer. Employing this platform, we have designed three sets of dopamine-modified ligands: Dopa-PIMA (compound **1**), Dopa-PIMA-PEG (compound **2**), and multi-reactive Dopa-PIMA-PEG-R (compound **3**), where R designates a laterally reactive group (see Figure 1).

Overall, this chemical design offers a few clear advantages: (1) The highly reactive maleic anhydride rings combined with the copolymer nature of the precursor allow effective coupling between PIMA and a variety of amine-presenting molecules. This permits one to introduce (in a one-step reaction) large but controlled numbers of anchoring, hydrophilic, and reactive functions, all in the same structures. (2) No additional reagents (e.g., DCC or EDC) are needed to facilitate the coupling; this also eliminates problems associated with ligand purification.[40] (3) This design can potentially be expanded to prepare additional platforms that are optimized for other nanoparticles including QDs and metal nanoparticles.

Synthesis and Characterization. Figure 1 shows a schematic representation of the general synthesis route used to prepare three sets of ligands. (1) Dopa-PIMA (compound **1**) is the simplest one and involved reacting activated dopamine with PIMA. Here, 50% of the maleic anhydride rings (∼20 units) in the polymer chain were targeted for reaction with dopamine, leaving the other 50% intact. The use of only a 50% mole fraction of dopamine allows a side-by-side comparison with the other PEGylated ligands (e.g., Dopa-PIMA-PEG) by providing the same number of dopamine groups per polymer platform during ligand exchange and the subsequent analysis. (2) The second set is Dopa-PIMA-PEG (compound **2**), which presents several PEG moieties and dopamine groups on the same platform. Typically, a total molar amount of aminated molecules equal to the molar concentration of maleic anhydride groups is used, with a 50:50 mixture of dopamine and H_2N-PEG-OMe. This is expected to introduce a total of ∼39 dopamines and PEG moieties, while freeing ∼39 carboxy groups along the polymer chain, which ensures that there are enough anchoring groups for effective coordination onto the NP surface and PEG segments for enhanced affinity to buffer media.[26,39,41,42] (3) The third set of ligands, Dopa-PIMA-PEG-R (compound **3**), contains a stoichiometric mixture of dopamine, methoxy-PEG, and reactive-PEG groups. This was achieved by replacing a fraction of the amine-PEG-OMe with amine-PEG-R during the addition reaction. For instance, by substituting 10−30% of the H_2N-PEG-OMe (used to prepare compound **2**) with H_2N-PEG-R during the substitution/addition reaction, a set of reactive polymer ligands, Dopa-PIMA-PEG-R, with ∼4 to 12 reactive functions was prepared (Figure 1). We should note that the nucleophilic addition reaction between maleic anhydride and aminated-PEG and dopamine could be completed within a few hours (4−8 h), though overnight reactions were used in the present study.

To address the poor reactivity of dopamine hydrochloride, we first activated the salt by adding an equimolar amount of triethylamine in dry DMF for 2 h, followed by centrifugation to remove insoluble salt (e.g., triethylamine hydrochloride). Carrying out the activation and addition reaction in subsequent steps is more effective than simply mixing the dopamine hydrochloride and triethylamine with the PIMA in the same solution. This improves the overall yield of the coupling reaction. Indeed, we found that when preparing the Dopa-PIMA ligand, the starting PIMA solution was slightly cloudy but gradually became homogeneous and colorless after ∼1 h of addition of activated dopamine.

Finally, we should note that the physical state of the three ligands after purification is influenced by the nature of the substituted groups. The reaction yielded a white powder for the purified Dopa-PIMA and a viscous yellowish oil for the Dopa-PIMA-PEG ligand (see Figure 1). The final yield of the addition reaction was slightly higher for compound **1**, with 91% yield measured for compound **1** and about 76% for compounds **2** and **3**.

The ligands were characterized using ^{1}H NMR spectroscopy. The ^{1}H NMR spectra for all three ligands (in DMSO-d_6) show a multiplet peak at 6.4−6.7 ppm (attributed to the aromatic protons from catechol). They also show a broad peak around 0.9 ppm ascribed to protons of methyl groups in the polymer (see Figure 1 and Supporting Information, Figures S2 and S3). The stoichiometry of the ligands for each compound was estimated from the corresponding ^{1}H NMR spectrum by comparing the relative integrations of the hydrogen peaks from the two methyl groups in the repeat units ($\delta \approx 0.9$ ppm, 234 H) and the three aromatic protons per catechol (δ = 6.4−6.7 ppm). From the integration, we measured ∼19 dopamines (57.72 H) per ligand for compound **1**, a value consistent with the total number of maleic anhydride rings in the PIMA precursor and the fact that only a 50% mole fraction of those were targeted for coupling (see Supporting Information, Figure S2). For compound **2** (Dopa-PIMA-PEG), the ^{1}H NMR spectrum showed a strong peak at 3.5 ppm (emanating from the PEG moieties) and a sharp peak at 3.23 ppm (from the methoxy groups), in addition to the multiplet at 6.4−6.7 ppm. An analysis of the integration of the above NMR peaks in the Dopa-PIMA-PEG spectrum provided estimates for the number of dopamine and PEG moieties grafted along the PIMA backbone. We measured an average of ∼19 dopamine groups (56−57 H) and ∼20 PEG-OMe moieties (61−62 H) per polymer chain (Figure 1). Overall, the above analysis indicates that the coupling efficiency between maleic anhydride and amino-containing molecules (here dopamine and H_2N-PEG-OMe) is essentially 100% complete. We should note that the number of dopamine groups measured for the present Dopa-PIMA-based ligands is much greater than that for OligoPEG-Dopa ligand (∼6 dopamines per chain) that we reported earlier using poly(acrylic acid) as a precursor polymer.[40] This is true even if we account for the difference in molecular weights between the two polymer precursors used (PAA has an index of

dx.doi.org/10.1021/la500974r | Langmuir 2014, 30, 6197−6208

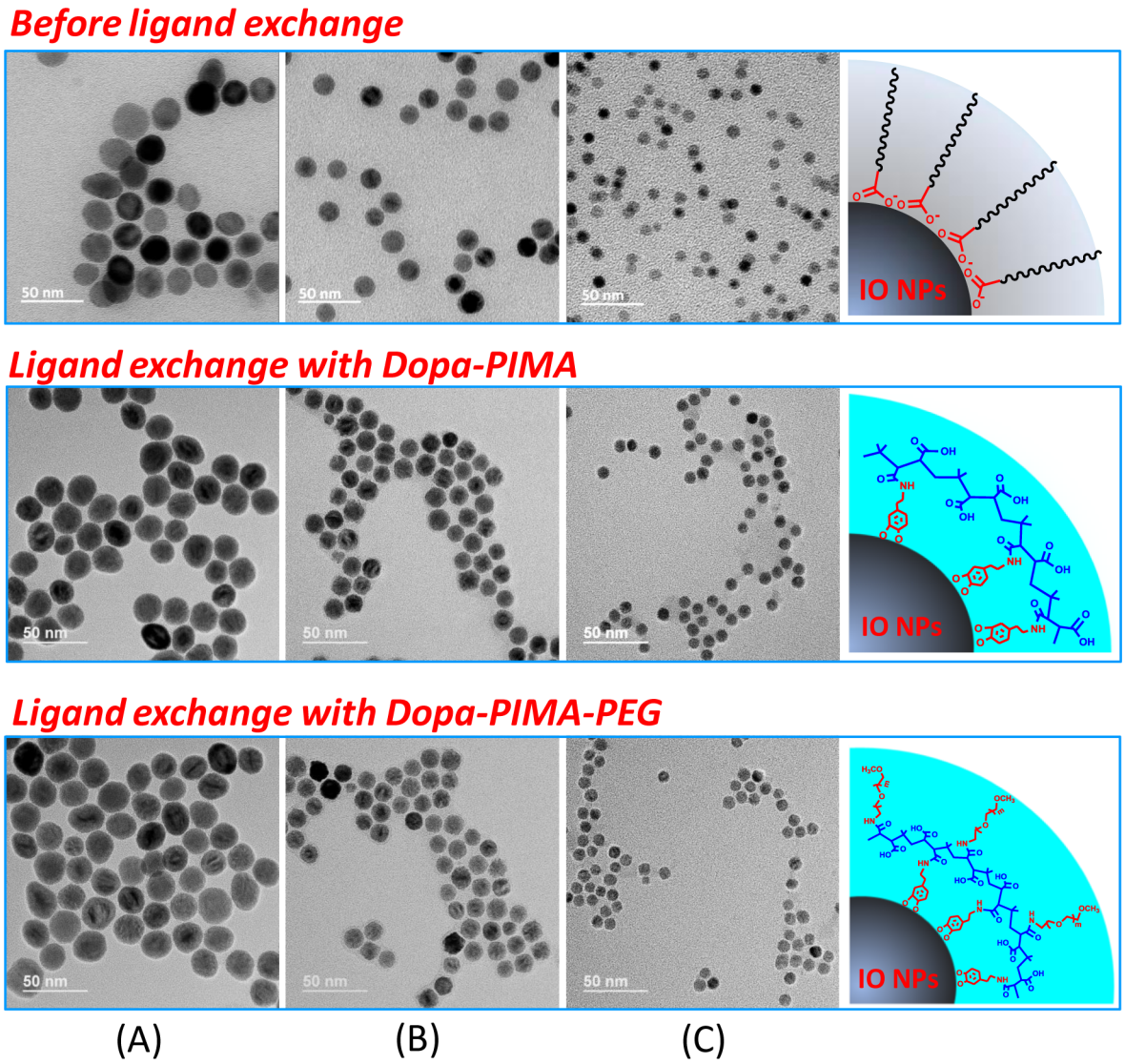

Figure 2. TEM images of iron oxide nanoparticles with 10.5 nm (A), 8.0 nm (B), and 4.6 nm (C) core radii before and after ligand exchange with Dopa-PIMA and Dopa-PIMA-PEG, respectively. Schematic illustrations of the nanoparticles with the corresponding surface capping ligands are also shown.

polymerization of 25), which confirms the advantages offered by the new platform for the synthesis of multidentate ligands.

Ligand Exchange and Characterization of Aqueous Fe_3O_4 NP Dispersions. Three different sets of Fe_3O_4 NPs capped with oleic acid, with an average radius, R_0, of 10.5, 8.0, and 4.6 nm (extracted from transmission electron microscopy, TEM experiments), were synthesized using the thermolysis of iron precursors as reported previously.[15] The TEM images shown in Figure 2 indicate that these nanoparticles are spherical, with uniform cores and a reduced size distribution. The nanoparticles were ligated with these polymers via mixing with the oleic acid-capped Fe_3O_4 NPs in THF overnight at 50 °C, followed by purification. Room temperature can also be used, but a longer incubation time may be needed. The nanoparticles capped with the new ligands were readily dispersible in water. An additional purification step to remove excess free ligands and solubilized oleic acid was carried out using a membrane filtration device (see Experimental Section). The TEM micrographs showed that nanoparticles capped with Dopa-PIMA or Dopa-PIMA-PEG maintain their overall size after surface modification with no sign of shape change or aggregation (see Figure 2). Ligand exchange with these amphiphilic polymers is also highly efficient and results in minimal to no loss (less than 10%) of materials after the phase transfer to water.

Dynamic light scattering (DLS) data indicate that after ligand exchange the nanoparticles have a narrow size distribution with low polydispersity index values (PDI $\leq$ 0.1), see Figure 3; representative plots of the autocorrelation function are provided in the Supporting Information, Figure S4. The hydrodynamic radii (R_H) measured for the three dispersions of Fe_3O_4 NPs capped with the native oleic acid in toluene were 16.7, 13.1, and 7.9 nm, respectively (Figure 3). This indicates that the ratio of sizes extracted from DLS and TEM, R_H/R_0, is ~1.5−1.6, in agreement with what is expected for such hard spheres and consistent with data reported for other materials.[43] The corresponding hydrodynamic sizes measured for NPs capped with Dopa-PIMA dispersed in water were 22.0, 19.2, and 14.4 nm, while those sizes measured for NPs capped with Dopa-PIMA-PEG were equal to 24.6, 20.6, and 15.3 nm, respectively (Figure 3). The phase transfer using these Dopa-PIMA-based ligands increases the hydrodynamic size of the IO

dx.doi.org/10.1021/la500974r | Langmuir 2014, 30, 6197−6208

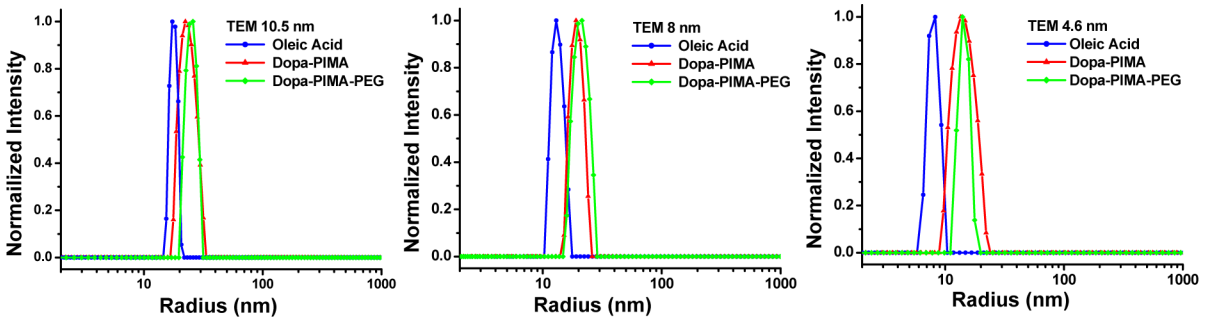

Core Radius, R_0 (nm), from TEM	Oleic Acid-capped		Dopa-PIMA-capped		Dopa-PIMA-PEG-capped	
	R_H(nm)	PDI	R_H(nm)	PDI	R_H(nm)	PDI
10.5	16.7	0.04	22.0	0.06	24.6	0.05
8.0	13.1	0.08	19.2	0.10	20.6	0.12
4.6	7.9	0.09	14.4	0.10	15.3	0.09

Figure 3. Histograms showing the distribution of the intensity vs hydrodynamic radius, extracted from the Laplace transform of the intensity autocorrelation function measured for the iron oxide nanoparticles capped with: oleic acid, Dopa-PIMA and Dopa-PIMA-PEG (top); a representative set of DLS autocorrelation functions is shown in the Supporting Information, Figure S4. Also shown are R_H values along with the corresponding polydispersity index (PDI) values for the various NPs before (oleic acid-capped dispersion in toluene) and after ligand exchange with Dopa-PIMA (compound **1**) and Dopa-PIMA-PEG (compound **2**), dispersed in DI water (bottom).

NPs by ~6−7 nm. The effects of introducing PEG groups added ~2 nm to the measured size on average compared to that of Dopa-PIMA ligands. This increase is significantly smaller than those measured for IO NPs surface functionalized with a silica shell or an organic cap made of either dextran or poly(vinylpyrrolidone) (PVP).[6,44,45] They are also smaller than those measured for NPs capped with monodopamine-PEG ligands having the same chain length.[46] This is likely due to the presence of some small aggregates in the monodopamine-PEG-capped NPs; these ligands cannot confer the same long-term colloidal stability to the NPs as multidentate dopamine ligands (e.g., Dopa-PIMA-PEG) are able to do.

Colloidal Stability Tests. Here, we show stability tests of aqueous dispersions of Dopa-PIMA- and Dopa-PIMA-PEG-capped nanoparticles (10.5 nm radius) in phosphate buffers at different pH values in the presence of 1 M NaCl and when mixed with growth media. Similar results were obtained for the other sets of NPs. The images shown in Figure 4B indicate that dispersions of NPs capped with Dopa-PIMA-PEG are colloidally stable over the pH range from 4 to 12 and in the presence of 1 M NaCl for at least 6 months of storage. After 6 months, IO NPs at pH 4 started to exhibit aggregation, and macroscopic precipitation occurred after 1 year of storage. These dispersions stayed stable at pH 6−12 and in the presence of 1 M NaCl for at least 1 year of storage. In comparison, dispersions of NPs capped with PEG-free ligand (e.g., Dopa-PIMA-NPs) progressively precipitated out of the solution at 1 M NaCl after 1 month of storage, along with partial aggregation observed after varying storage times for pH 4−8. For instance, dispersions of Dopa-PIMA-NPs at pH 4 started to aggregate after 3 months, but no aggregate formation was observed until 1 year at pH 8 (Figure 4A). Colloidal stability data of IO NPs capped with these two ligands in 100% growth media (RPMI-1640) are shown in Figure 4C. The dispersion stayed stable and aggregate-free for at least 1 month.

The DLS measurements further complement the above colloidal stability data. The graphs shown in Figure 4D,E indicate that while a fixed hydrodynamic size was measured for the Dopa-PIMA-PEG-capped NPs (Dopa-PIMA-NPs) across the full pH range and in 1 M NaCl for the 3-month test period, a sizable increase in R_H was measured for Dopa-PIMA-NPs in pH 4 buffer and in 1 M NaCl solution. At pH 4, the hydrodynamic size of Dopa-PIMA-NPs progressively increased from ~22 to ~29 nm after 1 month and to 39 nm after 3 months. Similarly, R_H increased to about 60 nm for Dopa-PIMA-NPs dispersed in 1 M NaCl after 1 month of storage. The weaker stability of Dopa-Dopa-PIMA-NPs may be attributed to the protonation of the carboxylic groups at lower pH and the screening of the electrostatic repulsions by counterions in the presence of 1 M NaCl. This confirms that for these PEG-free ligands, colloidal stabilization of the NPs is driven by electrostatic repulsions. However, incorporating PEG moieties into polymer ligand expands the range of colloidal stability conditions. Similar long-term stability data with respect to pH changes and in the presence of excess salt were collected for nanoparticles of other sizes. We would like to compare our findings to those achieved using ligand exchange with mono-Dopa-PEG described in ref 40, where limited stability was measured; in those experiments, precipitation took place after 1 day at pH 4 and after 1 month at pH 11. NPs capped with oligo-PEG-Dopa presenting ~6 dopamines per chain were stable for 1 month at pH 4 and 12 and for 2 months in 1 M NaCl solution.[40]

Nanoparticle Functionalization. The direct attachment of biomolecules to NP surfaces, driven by metal coordination, has been applied to attach peptides, proteins, and DNA to Au

dx.doi.org/10.1021/la500974r | Langmuir 2014, 30, 6197−6208

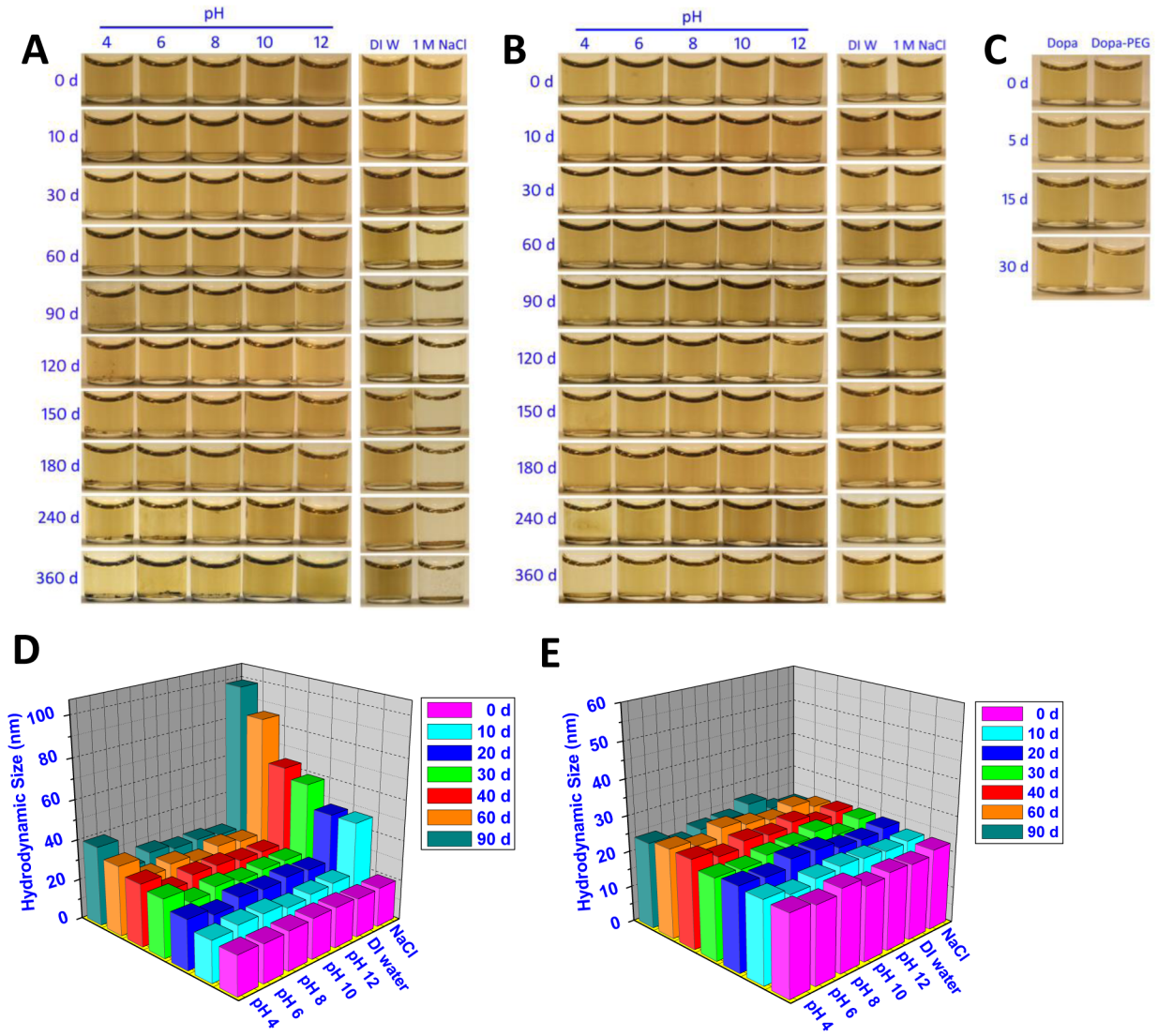

Figure 4. Colloidal stability tests of iron oxide nanoparticles (10.5 nm in radius) ligand exchanged with Dopa-PIMA (A) and Dopa-PIMA-PEG (B) dispersed in phosphate buffer (50 mM) from pH 4 to 12 and in the presence of excess electrolyte (1 M NaCl). The concentration of nanoparticles is ~20 μg/mL. (C) Stability tests of iron oxide nanoparticle dispersions in 100% cell growth media: Dopa-PIMA-NPs (left) and Dopa-PIMA-PEG-capped NPs (right). (D and E) Time progression of the hydrodynamic radius of iron oxide nanoparticles ligand exchanged with Dopa-PIMA and Dopa-PIMA-PEG, respectively.

nanoparticles and QDs. In particular, a variety of thiol-modified oligonucleotides and peptides have been immobilized on Au nanoparticles and QDs.[47] Similarly, polyhistidine-tagged proteins and peptides have also been immobilized on QD surfaces.[48] However, the direct use of such a strategy to attach biomolecules to iron oxide NPs has been much less effective. The conjugation of biomolecules to NPs via electrostatic interactions has been reported,[49] but this mode of coupling is sensitive to pH, soluble ions, and proteins in the medium.[19] The covalent linking of biomolecules to functional groups on the NP surface is thus preferable, and commonly suitable groups include amines, carboxylic acids, and thiols.[19,50] They can be used for implementing coupling strategies such as carboxyl-to-amine or thiol-to-amine (via a maleimide linker).[19]

With the robustness and compactness of Dopa-PIMA-PEG-capped NPs established, we turned our attention to the goal of incorporating chemical functionalities into the ligand. This can be achieved in the present design by simply replacing a fraction of the methoxy-terminated amino-PEG (H_2N-PEG-OMe) with terminally reactive moieties (H_2N-PEG-R with R = azide, amine, or lipoic acid). For example, using a mixture of 15:35 H_2N-PEG-N_3:H_2N-PEG-OMe (as a percentage) during the addition reaction, we prepared an azide-modified ligand with ~6 azide groups per chain. This can provide NPs that are compatible with azide−alkyne cycloaddition (CLICK) coupling to target biomolecules, including DNA, peptides, and proteins.[50] We have also prepared thiol-modified Dopa-PIMA-PEG ligands by substituting a fraction of H_2N-PEG-OMe with H_2N-PEG-LA during the addition reaction. The reduction of the LA groups (e.g., chemically) would provide thiol-presenting polymer ligands. The insertion of azide and lipoic acid was verified using FT-IR and ^{1}H NMR spectroscopy, respectively. For instance, the FTIR spectrum of Dopa-PIMA-PEG-azide showed a clearly defined vibrational band at 2108 cm^{-1} (ascribed to azide), while the multiple peaks at 1.3−2.4 and 3.1−3.2 ppm measured in the ^{1}H NMR spectrum of the Dopa-PIMA-PEG-LA ligand are ascribed to the lipoic acid

dx.doi.org/10.1021/la500974r | Langmuir 2014, 30, 6197−6208

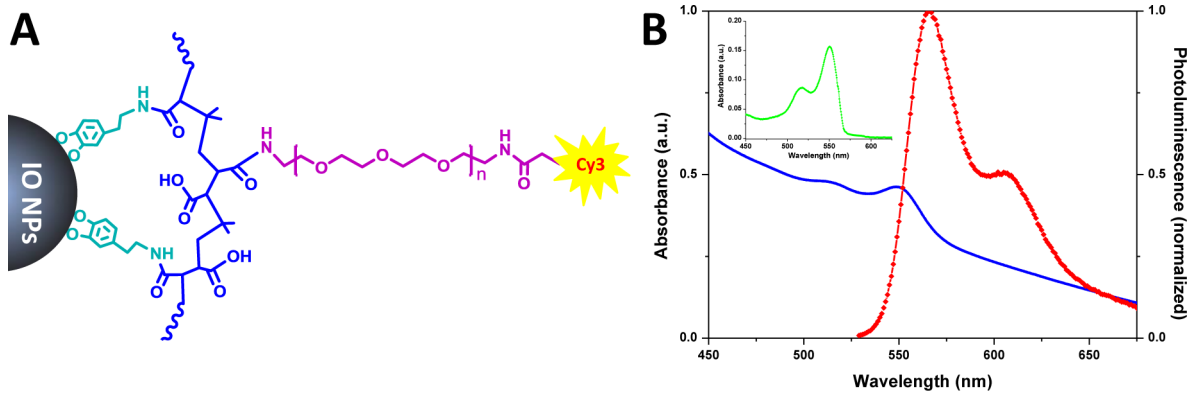

Figure 5. (A) Covalent conjugation of amine-functionalized NPs with sulfo-Cy3 NHS-ester dye. (B) Absorption (blue) and emission (red) spectra of the purified conjugates. The inset shows the deconvoluted absorption spectrum of Cy3 (green).

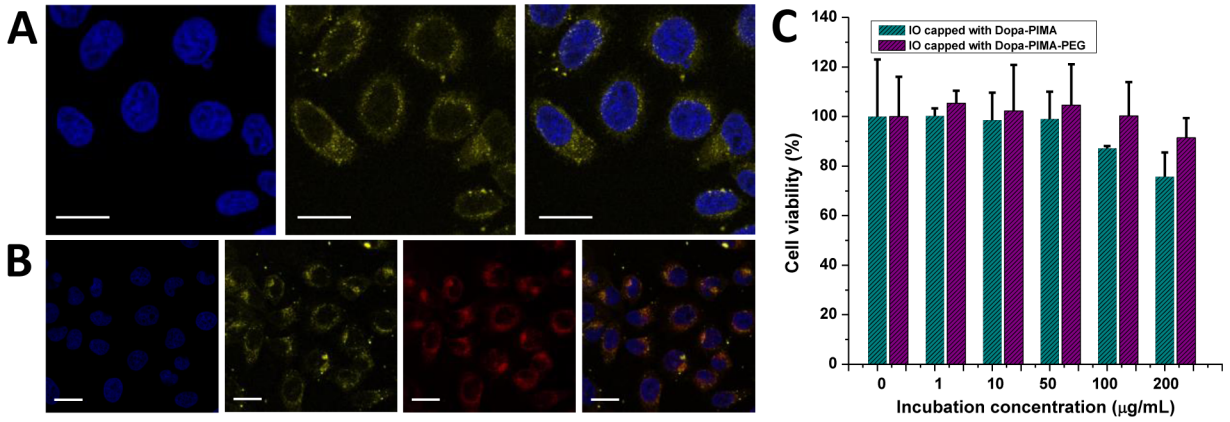

Figure 6. (A) Confocal laser scanning microscopy images of HeLa cells incubated with Fe_3O_4-Cy3 for 1 h. Upper left: Nuclei stained with blue 4′-6-diamidino-2-phenylindole (DAPI). Upper middle: Spotlike yellow fluorescence showing internalized Fe_3O_4-Cy3. Upper right: Merged image of blue (DAPI) and yellow (Fe_3O_4-Cy3) signals. Scale bar = 20 μm. (B) Confocal laser scanning microscopy images of HeLa cells incubated with Fe_3O_4-Cy3 conjugates and transferrin-Cy5 (as an endosome-specific marker) for 1 h. The distribution of patterns containing Fe_3O_4-Cy3 (yellow, lower panels) was colocalized with those of Cy5-transferrin (red, lower panels). Scale bar = 20 μm. (C) MTT viability test of HeLa cells incubated with varying concentrations of Fe_3O_4 NP capped with the PIMA-based ligands. NPs with a 10.5 nm radius have been used.

protons; additional details are provided in the Supporting Information (Figure S3).

The synthesis of the Dopa-PIMA-PEG-amine ligand was carried out using a small modification to minimize potential problems associated with cross-linking that may be caused by the reaction of the two amine groups in a H_2N-PEG-NH_2 chain with anhydride rings on separate polymer backbones. The nucleophilic addition reaction was carried out in two steps: the mixture of dopamine and H_2N-PEG-OMe was first added to PIMA solution, and then after 3 h, the desired amount of H_2N-PEG-NH_2 (e.g., 15%) was added. To prove that this route provides amine-reactive Fe_3O_4 NPs, we conjugated NHS-ester-modified sulfo-Cy3 to NPs ligand-exchanged with Dopa-PIMA-PEG-amine (15% amine). Figure 5 shows the absorption and emission spectra collected from the Fe_3O_4-Cy3 conjugates after purification. There is a clear contribution from the dye to the measured absorption spectrum at 549 nm and a well-defined fluorescence signature with a maximum at 566 nm; both are characteristic of the Cy3 dye (see inset in Figure 5).

Cell Imaging. Figure 6 shows a representative set of fluorescent images collected from HeLa cells incubated with the Fe_3O_4-Cy3 conjugates; images show the distribution of cell nuclei, stained with DAPI (blue, upper panel 1), and the yellow signal associated with the distribution of Fe_3O_4-Cy3 (upper panel 2), together with the Cy5-transferrin (red) as a late endolysosomal marker (lower panel 3). These images show that the yellow fluorescence from the Fe_3O_4-Cy3 conjugates is dispersed throughout the cell cytoplasm and none is found in the nucleus. They also show that the yellow conjugates are mostly colocalized with the distribution of endo/lysosomal compartments (see yellow and red superposed images shown in lower panel 4), indicating that Fe_3O_4-Cy3 has been primarily internalized via endocytosis. This type of nonreceptor-mediated endocytosis is observed frequently in HeLa cells and seems to be a general process occurring in various cells upon ingestion of nanoparticles without having surface-grafted agonists; longer incubation times and rather high concentrations of reagents (e.g., μM for QDs) are needed, nonetheless.[45,51,52]

In Vitro Cytotoxicity Evaluation. We assessed the cytotoxicity of the Dopa-PIMA- and Dopa-PIMA-PEG-stabilized Fe_3O_4 nanoparticles (10.5 nm radius) using an MTT (3-(4,5-dimethylthiazol-2-yl)-2,5-diphenyltetrazolium bromide) assay on the human cervix carcinoma cell line (HeLa cell). Figure 6C shows that the viability of cells incubated with Dopa-PIMA-PEG-Fe_3O_4 NPs essentially remained at 100% throughout the range of concentrations used. In comparison, the viability of cells incubated with Dopa-PIMA-capped Fe_3O_4 NPs slightly decreased to 70−80% at reagent concentrations exceeding 100−200 μg/mL. These results indicate that overall NPs capped with the polymer ligand

dx.doi.org/10.1021/la500974r | Langmuir 2014, 30, 6197−6208

containing PEG moieties induces minimal to no toxicity to cell cultures. This result is consistent with other measurements showing the marginal toxicity of iron oxide NPs to various cells.

Relaxivity Measurements. The accumulation of IO NPs within tissues results in strong contrast effects in MRI scans. When dispersed in aqueous solutions or in a biological tissue and in the presence of an external magnetic field, the superparamagnetic NPs create microscopic field inhomogeneities that affect the spins of neighboring water molecules.[5,53] The diffusion of water molecules into these zones of magnetic inhomogeneities affects a large number of water molecules, inducing the activation of spin dephasing (contrast effect) which is primarily measured as a shortening of the spin−spin relaxation times (T_2) or an increase in the spin−spin relaxation rates (r_2). The size of the IO NP plays a key role in the effective contrast values. On the nanoscale, single magnetic domains are developed, and each has a corresponding magnetic moment that is aligned in a particular direction defined by the magnetic anisotropy values of the NP. Within the range of 1−20 nm, surface spins tend to be slightly tilted, forming a magnetically disordered spin-glass-like "surface layer".[53] This surface effect significantly influences the magnetic moments and in turn alters the T_2 relaxation of neighboring water molecules. Moreover, this effect is strongly dependent on the NP size.[18,53] As the size decreases, the surface effect becomes more pronounced, resulting in the reduced net magnetic moment and therefore influencing the spin−spin relaxation (r_2) of the water protons. The general trend is that as the size of the IO NP increases, the T_2 relaxation time at the same concentration decreases and r_2, defined as the slope of $1/T_2$ against Fe concentration, increases.[18] IO NPs with higher r_2 values exhibit detectable T_2 changes and a contrast effect with fewer nanoparticles as opposed to IO NPs with lower r_2 values. Thus, we reasoned that the r_2 values of the IO NPs with a radius of 10.5 nm should be larger than that of those IO NPs with a smaller radius. Plots of the relaxation rates ($1/T_2$) for the corresponding Fe_3O_4 NPs capped with the various Dopa-PIMA-modified ligands as a function of Fe concentration show linear behavior for all of the samples tested (see Supporting Information, Figure S5). Furthermore, the r_2 value for the Dopa-PIMA-PEG-capped IO NPs increased from 68.6 to 109.1 and 172.0 mM^{-1} s^{-1} as the size changed from 4.6 to 8.0 and then 10.5 nm (Table 1).

Table 1. Relaxivity Values Extracted from Plots of the T_2 relaxation Time vs NP Concentration (Shown in the Supporting Information) of Dopa-PIMA- and Dopa-PIMA-PEG-Stabilized Fe_3O_4 Nanoparticles with the Three Different Sizes: 4.6, 8.0, and 10.5 nm[a]

core radius, R_0 (nm), from TEM	r_2 (mM^{-1} s^{-1}) Dopa-PIMA-capped	r_2 (mM^{-1} s^{-1}) Dopa-PIMA-PEG-capped
4.6	40.1	68.6
8.0	118.2	109.1
10.5	193.7	172.0

[a]The raw data shown for the $1/T_2$ vs Fe concentration of Fe_3O_4 NPs are provided in the Supporting Information, Figure S5.

Similarly, the r_2 values rose from 40.1 to 118.2 and 193.7 mM^{-1} s^{-1} for Dopa-PIMA-capped IO NPs as the nanoparticle size increased. These IO NP core-size-dependent r_2 values are comparable to or even greater than those reported for other Fe_3O_4-type magnetic nanoparticles in the literature.[6,44,54]

CONCLUSIONS

We have designed a new class of multicoordinating amphiphilic polymers ideally adapted for surface-functionalizing iron oxide nanoparticles. The ligand design relies on the specific and highly efficient nucleophilic addition between amine and maleic anhydride. Using this scheme, we were able to insert controllable numbers of amine-presenting anchoring hydrophilic and reactive groups onto a poly(isobutylene-*alt*-maleic anhydride) chain using a one-step reaction and without the need for additional coupling reagents or excess amine-presenting precursors. This provided a set of polymer ligands that present multiple dopamine anchors along with several hydrophilic and reactive PEG moieties. The ligand exchange of hydrophobic iron oxide nanoparticles with these ligands is rapid and provides aggregate-free hydrophilic dispersions of NPs with great long-term colloidal stability over a broad range of pH values (pH 4−12) and in the presence of a large excess of electrolytes, as verified by light-scattering measurements and the stability in growth media. The hydrophilic nanoparticles are compact in size and reactive with target molecules. We have also assembled an MRI-optical dual-mode probe via covalent conjugation of amine-functionalized Fe_3O_4 NPs with sulfo-Cy3 NHS ester dye and utilized them in the fluorescent imaging of live cells with good biodistribution. Furthermore, T_2 relaxation measurements of these dispersions showed that the relaxivity coefficient, r_2, for these materials exhibits a consistent magnetic resonance enhancement with nanocrystal size. This opens up the possibility for using these magnetic platforms as MRI contrast agents to image cells and tissues and for designing specific biosensors. These materials can be easily integrated into the design of additional multimodal platforms. Finally, we stress that the present ligand design can be easily adapted to a variety of other inorganic nanocrystals, such as quantum dots and metal nanoparticles. Some of those approaches are being explored in our laboratory and will be discussed in future work(s).

EXPERIMENTAL SECTION

Synthesis of Dopamine-Modified PIMA (Dopa-PIMA, Compound 1). In a 50 mL three-necked round-bottomed flask equipped with an addition funnel and a magnetic stirring bar, 0.385 g of poly(isobutylene-*alt*-maleic anhydride) (PIMA, $M_w \approx 6000$ g/mol, 2.5 mmol monomer units) was dissolved in 10 mL of DMF. The flask was purged with nitrogen for 10−15 min, and the solution was heated to 70 °C. In a separate vial, 0.237 g of dopamine hydrochloride (1.25 mmol) was dissolved in 2 mL of DMF, to which an equivalent molar amount of triethylamine was added. The solution became turbid and was stirred for 2 h at room temperature under a nitrogen atmosphere to allow for dopamine activation, followed by centrifugation to remove the formed salts (e.g., triethylamine hydrochloride). The supernatant was loaded into the additional funnel and added dropwise to the flask containing the PIMA solution. Once the addition was complete, the reaction mixture was stirred overnight at 70 °C. After the DMF was removed under vacuum, DI water was added to precipitate the product, which was washed with 1 M HCl solution (three to four times), followed by a final rinse with DI water. Lyophilization of the solution yielded the product as a white powder.

Synthesis of Dopamine- and PEG-Modified PIMA (Dopa-PIMA-PEG, Compound 2). PIMA (0.385 g, 2.5 mmol monomer units) was dissolved in 10 mL of DMF in a 50 mL three-necked round-bottomed flask equipped with an additional funnel and a magnetic stirring bar. The solution mixture was purged with nitrogen and then heated to 70 °C. Separately, a mixture of amino-PEG (H_2N-PEG-OMe, 0.995 g, 1.25 mmol) and dopamine (0.237 g, 1.25 mmol) activated using triethylamine (as described above) was prepared in 4

dx.doi.org/10.1021/la500974r | Langmuir 2014, 30, 6197−6208

mL of DMF. This content was loaded into the addition funnel and then added dropwise to the PIMA solution. When the addition was complete, the reaction mixture was further stirred at 70 °C overnight. The DMF was removed under vacuum, and then 3 mL of chloroform was added. The solution was purified by silica column chromatography using chloroform as the eluent. Following solvent evaporation, a gel-like yellow oil was collected as the final product.

Synthesis of Reactive Dopa-PIMA-PEG (Dopa-PIMA-PEG-R, Compound 3). Here we follow the same synthesis steps used for preparing Dopa-PIMA-PEG above but substitute a fraction of H_2N-PEG-OMe with H_2N-PEG-R (R is an azide or a disulfide). We briefly describe the synthesis of azide-functionalized Dopa-PIMA-PEG. Poly(isobutylene-*alt*-maleic anhydride) (0.385 g, 2.5 mmol monomer units) was dissolved in 10 mL of DMF and loaded into a 50 mL three-necked round-bottomed flask equipped with an addition funnel. The flask was purged with nitrogen, and the solution was heated to 70 °C. A separately prepared mixture of dopamine (0.375 g, 1.25 mmol) activated with triethylamine, H_2N-PEG-OMe (0.70 g, 0.875 mmol), and H_2N-PEG-N_3 (0.247 g, 0.375 mmol) dissolved in 4 mL of DMF was loaded into the addition funnel and then added dropwise to the polymer solution. The reaction mixture was stirred overnight at 70 °C under nitrogen. After the DMF was removed under vacuum, 3 mL of chloroform was added, and the product was purified by silica column chromatography using chloroform as the eluent. The product as a yellow viscous liquid was obtained following solvent evaporation. Additional details on ligands with other functional groups are provided in the Supporting Information.

Synthesis of Iron Oxide Nanoparticles. We followed the synthesis scheme described in ref 15. Briefly, to synthesize the iron-oleate complex (i.e., precursor), 3.6 g of $FeCl_3{\cdot}6H_2O$ and 12.2 g of sodium oleate were dissolved in a solvent mixture made of 26 mL of ethanol, 20 mL of DI water, and 46 mL of hexane. The mixture was heated to 70 °C for 4 h. Then the upper layer containing the iron-oleate complex in hexane was washed with distilled water three times, and the hexane was evaporated, yielding the iron-oleate complex as a brown oil.

The growth of the iron oxide nanoparticles relied on the reduction of iron-oleate at high temperature. Briefly, 3.6 g of the Fe-oleate complex and 0.57 g of oleic acid were dissolved in 20 g of 1-octadecene. The mixture was heated (at a constant heating rate of 3.3 °C/min) to 320 °C, and then the solution was maintained at that temperature for 30 min; these conditions provided a dispersion of 8.0 nm (radius) iron oxide nanoparticles. Nanoparticles with additional sizes are grown by changing the annealing temperature, as previously described.[15]

Ligand Exchange of Fe_3O_4 Nanoparticles. A typical ligand exchange and phase transfer is carried out as follows. One milliliter of the growth dispersion in hexane was precipitated using ethanol. The turbid solution was centrifuged, and the supernatant was discarded, providing ∼5 mg of nanoparticles as a wet pellet. The precipitate containing the nanoparticles was dispersed in 0.5 mL of THF and then further mixed with 1 mL of THF containing 25 mg of solubilized Dopa-PIMA-PEG (compound **2**). The vial was sealed, and the atmosphere was switched to nitrogen and stirred overnight at 50 °C using an oil bath. The sample was precipitated using excess hexane and centrifuged at 3900 rpm for 4 min to provide a dark pellet. The clear supernatant was discarded, and the pellet was redissolved in a mixture of 0.5 mL of THF and 0.3 mL of ethanol, followed by precipitation by adding excess hexane. The turbid dispersion was centrifuged, the supernatant was discarded, and the residual precipitate was dried under vacuum to yield a dark pellet, which was easily dispersed by adding 1 to 2 mL of DI water. After sonication, the aqueous dispersion was filtered with a 0.45 μm disposable syringe filter, and then excess free ligands were removed by applying three to four rounds of concentration/dilution (DI water) using a centrifugal filtration device (Millipore, M_w cutoff = 100 kDa). A similar protocol was applied to ligand exchange with Dopa-PIMA-PEG-R. Ligand exchange with Dopa-PIMA followed the same steps described for Dopa-PIMA-PEG, but the ligand was dissolved in THF mixed with a few drops of ethanol and the dry pellet after ligand exchange was first dissolved in buffer (pH 8) with sonication.

Dynamic Light Scattering (DLS) Measurements. The hydrodynamic size of the iron oxide nanoparticles, either capped with their native ligands dispersed in toluene or cap-exchanged with Dopa-PIMA or Dopa-PIMA-PEG ligands (dispersed in buffer media, pH 7.5), was measured using an ALV/CGS-3 compact goniometer system. All of the dispersions were filtered through a 0.22 μm disposable filter (Millipore) before the scattered signal was collected. The signal was collected at angles varying between 60° and 120°. Each scattered pattern was the average result of three acquisition periods of 10 s each. The intensity count rates were maintained at ∼150−300 Hz, achieved through appropriate control of the NP concentrations for the various nanoparticle sizes used. The resulting autocorrelation function was fitted to a cumulant series using ALV-7004 correlator software. For every sample, we verified that the measured hydrodynamic size (extracted from the Laplace transform of the autocorrelation function) is independent of the scattering angle, as anticipated.[43,55] The data on the hydrodynamic size reported here were collected at a 90° scattering angle. To track possible changes in the NP size for a particular dispersion with time, the signal was collected and analyzed at different time intervals.

Covalent Conjugation of Sulfo-Cy3 NHS Ester to Polymer-Ligated Fe_3O_4 NPs. We detail the procedure for conjugating IO NPs (10.5 nm in radius) capped with amine-modified Dopa-PIMA-PEG (i.e., 15% of the PEG moieties had terminal amines) with sulfo-Cy3 NHS ester. Briefly, 200 μL of amine-functionalized NPs (amine-Fe_3O_4 NPs, concentration ∼2 mg/mL) was first dispersed in 300 μL of phosphate buffer (pH 7.5) and stirred for 1 h. Then a 5−8-fold excess of sulfo-Cy3 NHS ester initially dissolved in 50 μL of DMSO was added, and the mixture was left to react at room temperature for 2 h and then overnight at 4 °C. Excess unreacted dye was removed by size exclusion using a PD 10 column (GE Healthcare). The conjugate was characterized using absorption and fluorescence spectroscopy.

Fluorescence Imaging of Live Cells. HeLa cell cultures (human cervix carcinoma cell line, provided by the FSU cell culture facility) were grown at 37 °C in a humidified 5% CO_2 atmosphere at 37 °C as a monolayer in a complete growth medium (Dulbecco's Modified Eagle's Medium, DMEM, Cellgro); the medium was supplemented with 10% (v/v) fetal bovine serum (Gibco), 4.5 g/L glucose, L-glutamine, sodium pyruvate, 1% (v/v) antibiotic-antimycotic 100× (Gibco), and 1% (v/v) nonessential amino-acid solution 100× (Sigma). The above cells (8×10^4) were first seeded onto 18 mm circle microcover glasses (VWR) of 24-well microplates (CellStar, VWR), and the plates were placed in an incubator overnight to allow for cell attachment. After 24 h, the cells were then mixed with Cy3-labeled Fe_3O_4 NPs at a concentration of 150 μg/mL NP-Cy3 conjugates and left to incubate for 1 h before rinsing. After incubation, the cells were washed with PBS buffer two times, fixed with 3.7% paraformaldehyde, and stained with 4,6-diamino-2-phenylindole (Prolong Antifade mounting media with DAPI nuclear staining, from Invitrogen). When Cy5-transferrin as a specific endosome/lysosome marker was also used, cells were first incubated with Cy3-labeled Fe_3O_4 NPs at a concentration of 150 μg/mL for 1 h. Then, after rinsing and washing with PBS buffer to remove excess Cy3-Fe_3O_4 conjugate, Cy5-transferrin (at 40 μg/mL) was added to the culture and incubated for 1 h. The cells were then washed with PBS buffer two times, fixed with 3.7% paraformaldehyde, and stained with 4,6-diamino-2-phenylindole. Fluorescent images were acquired from the above cultures using a Leica SP2SE, DM600 confocal laser scanning microscope equipped with acousto-optic tunable filters (AOTF) for detection. The DAPI, Fe_3O_4-Cy3, and Cy5-transferrin were imaged using laser excitation at 405, 546, and 633 nm, respectively. The emission signals of DAPI, Fe_3O_4-Cy3, and Cy5-transferrin were collected in the optical ranges of 436−477, 560−590, and 663−705 nm, respectively.

Viability Assays. The viability of HeLa cells incubated with NPs capped with either Dopa-PIMA or Dopa-PIMA-PEG at concentrations of 0, 1, 10, 50, 100, and 200 μg/mL was tested using an MTT assay. The MTT assay is a colorimetric test based on the cellular reduction of

dx.doi.org/10.1021/la500974r | *Langmuir* 2014, 30, 6197−6208

3-(4,5-dimethylthiazol-2-yl)-2,5-diphenyl tetrazolium bromide (MTT, Sigma-Aldrich) by the mitochondrial dehydrogenase of viable cells, forming a blue formazan product which can be characterized spectrophotometrically. MTT solution was prepared at 5 mg/mL in PBS 1× and then diluted 1:5 in medium without serum or phenol red. Cells were first seeded into 96-well microplates (2×10^4 cells/200 μL/well), and the plates were placed in an incubator overnight to allow adherence. After 24 h, the nanoparticles were applied directly to the wells using a multichannel pipet (in triplicate), and the cultures were incubated for 24 h at 37 °C. After incubation, the medium was removed, the cells were washed twice with PBS 1×, and then 200 μL of the MTT solution (0.2 mg/mL) was added to each well. After 4 h of incubation at 37 °C, the MTT solution was removed and 100 μL of DMSO was added to each well to solubilize the MTT-formazan product. The absorbance at 560 nm was measured using the Infinite M1000 PRO plate reader (TECAN). The cell viability obtained from the absorbance measurements was expressed as a fraction of viable cells and normalized to that of cells that were not exposed to reagents.

MRI Relaxometry Measurements. The T_2 relaxation times of the corresponding IO NP suspensions were measured with a 0.47T mq20 NMR analyzer (Minispec, Bruker, Billerica, MA) using a CPMG pulse-echo train with a 1.5 ms interpulse spacing. For the determination of r_2 values, various dilutions of the corresponding IO NPs were prepared and their T_2 relaxation times were measured. Then a plot of the relaxation rates ($1/T_2$) vs the corresponding iron concentration was created. The slope for each of the plots corresponding to different IO NP preparations was the value of r_2. Iron concentrations for each of the NPs were determined spectrophotometrically after acid digestion of the nanoparticles' suspension as previously described.[1,13]

■ ASSOCIATED CONTENT

Ⓢ Supporting Information

Additional experimental details, including FTIR and NMR characterization of the ligands and T_2 relaxation values. This material is available free of charge via the Internet at http://pubs.acs.org.

■ AUTHOR INFORMATION

Corresponding Author

*Address correspondence to mattoussi@chem.fsu.edu.

Present Address

H.B.N.: Department of Chemical Engineering, Myongji University, Yongin, Gyeonggido 449-728, Korea.

Notes

The authors declare no competing financial interest.

■ ACKNOWLEDGMENTS

We thank FSU and the National Science Foundation for financial support (NSF-CHE no. 1058957). We also thank Fadi Aldeek for providing the Transferrin labeling marker and for fruitful discussions. We also thank the FSU TEM facility and Ruth Didier at the College of Medicine for assistance with confocal microscopy.

■ REFERENCES

(1) Lewin, M.; Carlesso, N.; Tung, C. H.; Tang, X. W.; Cory, D.; Scadden, D. T.; Weissleder, R. Tat peptide-derivatized magnetic nanoparticles allow in vivo tracking and recovery of progenitor cells. *Nat. Biotechnol.* **2000**, *18*, 410−414.

(2) Gupta, A. K.; Gupta, M. Synthesis and surface engineering of iron oxide nanoparticles for biomedical applications. *Biomaterials* **2005**, *26*, 3995−4021.

(3) Lee, J. H.; Huh, Y. M.; Jun, Y.; Seo, J.; Jang, J.; Song, H. T.; Kim, S.; Cho, E. J.; Yoon, H. G.; Suh, J. S.; Cheon, J. Artificially engineered magnetic nanoparticles for ultra-sensitive molecular imaging. *Nat. Med.* **2007**, *13*, 95−99.

(4) Jun, Y. W.; Lee, J. H.; Cheon, J. Chemical design of nanoparticle probes for high-performance magnetic resonance imaging. *Angew. Chem., Int. Ed.* **2008**, *47*, 5122−5135.

(5) Mattoussi, H.; Cheon, J. *Inorganic Nanoprobes for Biological Sensing and Imaging*; Artech House: Boston, 2009.

(6) Kim, J.; Piao, Y.; Hyeon, T. Multifunctional nanostructured materials for multimodal imaging, and simultaneous imaging and therapy. *Chem. Soc. Rev.* **2009**, *38*, 372−390.

(7) Frey, N. A.; Peng, S.; Cheng, K.; Sun, S. Magnetic nanoparticles: synthesis, functionalization, and applications in bioimaging and magnetic energy storage. *Chem. Soc. Rev.* **2009**, *38*, 2532−2542.

(8) Perez, J. M.; Josephson, L.; O'Loughlin, T.; Hogemann, D.; Weissleder, R. Magnetic relaxation switches capable of sensing molecular interactions. *Nat. Biotechnol.* **2002**, *20*, 816−820.

(9) Xu, C. J.; Xu, K. M.; Gu, H. W.; Zheng, R. K.; Liu, H.; Zhang, X. X.; Guo, Z. H.; Xu, B. Dopamine as a robust anchor to immobilize functional molecules on the iron oxide shell of magnetic nanoparticles. *J. Am. Chem. Soc.* **2004**, *126*, 9938−9939.

(10) Nasongkla, N.; Bey, E.; Ren, J. M.; Ai, H.; Khemtong, C.; Guthi, J. S.; Chin, S. F.; Sherry, A. D.; Boothman, D. A.; Gao, J. M. Multifunctional polymeric micelles as cancer-targeted, MRI-ultrasensitive drug delivery systems. *Nano Lett.* **2006**, *6*, 2427−2430.

(11) Medarova, Z.; Pham, W.; Farrar, C.; Petkova, V.; Moore, A. In vivo imaging of siRNA delivery and silencing in tumors. *Nat. Med.* **2007**, *13*, 372−377.

(12) El-Boubbou, K.; Zhu, D. C.; Vasileiou, C.; Borhan, B.; Prosperi, D.; Li, W.; Huang, X. F. Magnetic Glyco-Nanoparticles: A Tool To Detect, Differentiate, and Unlock the Glyco-Codes of Cancer via Magnetic Resonance Imaging. *J. Am. Chem. Soc.* **2010**, *132*, 4490−4499.

(13) Santra, S.; Kaittanis, C.; Grimm, J.; Perez, J. M. Drug/Dye-Loaded, Multifunctional Iron Oxide Nanoparticles for Combined Targeted Cancer Therapy and Dual Optical/Magnetic Resonance Imaging. *Small* **2009**, *5*, 1862−1868.

(14) Rockenberger, J.; Scher, E. C.; Alivisatos, A. P. A new nonhydrolytic single-precursor approach to surfactant-capped nanocrystals of transition metal oxides. *J. Am. Chem. Soc.* **1999**, *121*, 11595−11596.

(15) Park, J.; An, K. J.; Hwang, Y. S.; Park, J. G.; Noh, H. J.; Kim, J. Y.; Park, J. H.; Hwang, N. M.; Hyeon, T. Ultra-large-scale syntheses of monodisperse nanocrystals. *Nat. Mater.* **2004**, *3*, 891−895.

(16) Sun, S. H.; Zeng, H.; Robinson, D. B.; Raoux, S.; Rice, P. M.; Wang, S. X.; Li, G. X. Monodisperse MFe2O4 (M = Fe, Co, Mn) nanoparticles. *J. Am. Chem. Soc.* **2004**, *126*, 273−279.

(17) Yu, W. W.; Falkner, J. C.; Yavuz, C. T.; Colvin, V. L. Synthesis of monodisperse iron oxide nanocrystals by thermal decomposition of iron carboxylate salts. *Chem. Commun.* **2004**, *20*, 2306−2307.

(18) Jun, Y. W.; Huh, Y. M.; Choi, J. S.; Lee, J. H.; Song, H. T.; Kim, S.; Yoon, S.; Kim, K. S.; Shin, J. S.; Suh, J. S.; Cheon, J. Nanoscale size effect of magnetic nanocrystals and their utilization for cancer diagnosis via magnetic resonance imaging. *J. Am. Chem. Soc.* **2005**, *127*, 5732−5733.

(19) Zhang, F.; Lees, E.; Amin, F.; Gil, P. R.; Yang, F.; Mulvaney, P.; Parak, W. J. Polymer-Coated Nanoparticles: A Universal Tool for Biolabelling Experiments. *Small* **2011**, *7*, 3113−3127.

(20) Mattoussi, H.; Palui, G.; Na, H. B. Luminescent quantum dots as platforms for probing in vitro and in vivo biological processes. *Adv. Drug Delivery Rev.* **2012**, *64*, 138−166.

(21) Mout, R.; Moyano, D. F.; Rana, S.; Rotello, V. M. Surface functionalization of nanoparticles for nanomedicine. *Chem. Soc. Rev.* **2012**, *41*, 2539−2544.

(22) Ling, D.; Hyeon, T. Chemical design of biocompatible iron oxide nanoparticles for medical applications. *Small* **2013**, *9*, 1450−66.

(23) Kim, B. S.; Qiu, J. M.; Wang, J. P.; Taton, T. A. Magnetomicelles: Composite nanostructures from magnetic nanoparticles and cross-linked amphiphilic block copolymers. *Nano Lett.* **2005**, *5*, 1987−1991.

(24) Tromsdorf, U. I.; Bigall, N. C.; Kaul, M. G.; Bruns, O. T.; Nikolic, M. S.; Mollwitz, B.; Sperling, R. A.; Reimer, R.; Hohenberg,

H.; Parak, W. J.; Forster, S.; Beisiegel, U.; Adam, G.; Weller, H. Size and surface effects on the MRI relaxivity of manganese ferrite nanoparticle contrast agents. *Nano Lett.* **2007**, *7*, 2422−2427.
(25) Yu, W. W.; Chang, E.; Falkner, J. C.; Zhang, J. Y.; Al-Somali, A. M.; Sayes, C. M.; Johns, J.; Drezek, R.; Colvin, V. L. Forming biocompatible and nonaggregated nanocrystals in water using amphiphilic polymers. *J. Am. Chem. Soc.* **2007**, *129*, 2871−2879.
(26) Lin, C. A.; Sperling, R. A.; Li, J. K.; Yang, T. Y.; Li, P. Y.; Zanella, M.; Chang, W. H.; Parak, W. J. Design of an amphiphilic polymer for nanoparticle coating and functionalization. *Small* **2008**, *4*, 334−341.
(27) Pellegrino, T.; Manna, L.; Kudera, S.; Liedl, T.; Koktysh, D.; Rogach, A. L.; Keller, S.; Radler, J.; Natile, G.; Parak, W. J. Hydrophobic nanocrystals coated with an amphiphilic polymer shell: A general route to water soluble nanocrystals. *Nano Lett.* **2004**, *4*, 703−707.
(28) Lees, E. E.; Nguyen, T. L.; Clayton, A. H. A.; Muir, B. W.; Mulvaney, P. The Preparation of Colloidally Stable, Water-Soluble, Biocompatible, Semiconductor Nanocrystals with a Small Hydrodynamic Diameter. *ACS Nano* **2009**, *3*, 1121−1128.
(29) Wu, X. Y.; Liu, H. J.; Liu, J. Q.; Haley, K. N.; Treadway, J. A.; Larson, J. P.; Ge, N. F.; Peale, F.; Bruchez, M. P. Immunofluorescent labeling of cancer marker Her2 and other cellular targets with semiconductor quantum dots. *Nat. Biotechnol.* **2003**, *21*, 41−46.
(30) Mikhaylov, G.; Mikac, U.; Magaeva, A. A.; Itin, V. I.; Naiden, E. P.; Psakhye, I.; Babes, L.; Reinheckel, T.; Peters, C.; Zeiser, R.; Bogyo, M.; Turk, V.; Psakhye, S. G.; Turk, B.; Vasiljeva, O. Ferri-liposomes as an MRI-visible drug-delivery system for targeting tumours and their microenvironment. *Nat. Nanotechnol.* **2011**, *6*, 594−602.
(31) Boyer, C.; Whittaker, M. R.; Bulmus, V.; Liu, J. Q.; Davis, T. P. The design and utility of polymer-stabilized iron-oxide nanoparticles for nanomedicine applications. *NPG Asia Mater.* **2010**, *2*, 23−30.
(32) Xie, J.; Xu, C. J.; Xu, Z. C.; Hou, Y. L.; Young, K. L.; Wang, S. X.; Pourmond, N.; Sun, S. H. Linking hydrophilic macromolecules to monodisperse magnetite (Fe3O4) nanoparticles via trichloro-s-triazine. *Chem. Mater.* **2006**, *18*, 5401−5403.
(33) Amstad, E.; Gillich, T.; Bilecka, I.; Textor, M.; Reimhult, E. Ultrastable Iron Oxide Nanoparticle Colloidal Suspensions Using Dispersants with Catechol-Derived Anchor Groups. *Nano Lett.* **2009**, *9*, 4042−4048.
(34) Wei, H.; Insin, N.; Lee, J.; Han, H. S.; Cordero, J. M.; Liu, W. H.; Bawendi, M. G. Compact Zwitterion-Coated Iron Oxide Nanoparticles for Biological Applications. *Nano Lett.* **2012**, *12*, 22−25.
(35) Zhang, T. R.; Ge, J. P.; Hu, Y. X.; Yin, Y. D. A general approach for transferring hydrophobic nanocrystals into water. *Nano Lett.* **2007**, *7*, 3203−3207.
(36) Shukoor, M. I.; Natalio, F.; Ksenofontov, V.; Tahir, M. N.; Eberhardt, M.; Theato, P.; Schroder, H. C.; Muller, W. E.; Tremel, W. Double-stranded RNA polyinosinic-polycytidylic acid immobilized onto gamma-Fe_2O_3 nanoparticles by using a multifunctional polymeric linker. *Small* **2007**, *3*, 1374−1378.
(37) Liong, M.; Shao, H.; Haun, J. B.; Lee, H.; Weissleder, R. Carboxymethylated polyvinyl alcohol stabilizes doped ferrofluids for biological applications. *Adv. Mater.* **2010**, *22*, 5168−5172.
(38) Stewart, M. H.; Susumu, K.; Mei, B. C.; Medintz, I. L.; Delehanty, J. B.; Blanco-Canosa, J. B.; Dawson, P. E.; Mattoussi, H. Multidentate Poly(ethylene glycol) Ligands Provide Colloidal Stability to Semiconductor and Metallic Nanocrystals in Extreme Conditions. *J. Am. Chem. Soc.* **2010**, *132*, 9804−9813.
(39) Ling, D.; Park, W.; Park, Y. I.; Lee, N.; Li, F.; Song, C.; Yang, S. G.; Choi, S. H.; Na, K.; Hyeon, T. Multiple-Interaction Ligands Inspired by Mussel Adhesive Protein: Synthesis of Highly Stable and Biocompatible Nanoparticles. *Angew. Chem., Int. Ed.* **2011**, *50*, 11360−11365.
(40) Na, H. B.; Palui, G.; Rosenberg, J. T.; Ji, X.; Grant, S. C.; Mattoussi, H. Multidentate catechol-based polyethylene glycol oligomers provide enhanced stability and biocompatibility to iron oxide nanoparticles. *ACS Nano* **2012**, *6*, 389−399.
(41) Uyeda, H. T.; Medintz, I. L.; Jaiswal, J. K.; Simon, S. M.; Mattoussi, H. Synthesis of compact multidentate ligands to prepare stable hydrophilic quantum dot fluorophores. *J. Am. Chem. Soc.* **2005**, *127*, 3870−3878.
(42) Nikolic, M. S.; Krack, M.; Aleksandrovic, V.; Kornowski, A.; Forster, S.; Weller, H. Tailor-made ligands for biocompatible nanoparticles. *Angew. Chem., Int. Ed.* **2006**, *45*, 6577−6580.
(43) Pons, T.; Uyeda, H. T.; Medintz, I. L.; Mattoussi, H. Hydrodynamic dimensions, electrophoretic mobility, and stability of hydrophilic quantum dots. *J. Phys. Chem. B* **2006**, *110*, 20308−20316.
(44) Lee, N.; Hyeon, T. Designed synthesis of uniformly sized iron oxide nanoparticles for efficient magnetic resonance imaging contrast agents. *Chem. Soc. Rev.* **2012**, *41*, 2575−2589.
(45) Huang, J.; Bu, L. H.; Xie, J.; Chen, K.; Cheng, Z.; Li, X. G.; Chen, X. Y. Effects of Nanoparticle Size on Cellular Uptake and Liver MRI with Polyvinylpyrrolidone-Coated Iron Oxide Nanoparticles. *ACS Nano* **2010**, *4*, 7151−7160.
(46) Xie, J.; Xu, C.; Kohler, N.; Hou, Y.; Sun, S. Controlled PEGylation of monodisperse Fe_3O_4 nanoparticles for reduced non-specific uptake by macrophage cells. *Adv. Mater.* **2007**, *19*, 3163−3166.
(47) Mirkin, C. A.; Letsinger, R. L.; Mucic, R. C.; Storhoff, J. J. A DNA-based method for rationally assembling nanoparticles into macroscopic materials. *Nature* **1996**, *382*, 607−609.
(48) Clapp, A. R.; Medintz, I. L.; Mauro, J. M.; Fisher, B. R.; Bawendi, M. G.; Mattoussi, H. Fluorescence resonance energy transfer between quantum dot donors and dye-labeled protein acceptors. *J. Am. Chem. Soc.* **2004**, *126*, 301−310.
(49) Mattoussi, H.; Mauro, J. M.; Goldman, E. R.; Anderson, G. P.; Sundar, V. C.; Mikulec, F. V.; Bawendi, M. G. Self-assembly of CdSe-ZnS quantum dot bioconjugates using an engineered recombinant protein. *J. Am. Chem. Soc.* **2000**, *122*, 12142−12150.
(50) Sapsford, K. E.; Algar, W. R.; Berti, L.; Gemmill, K. B.; Casey, B. J.; Oh, E.; Stewart, M. H.; Medintz, I. L. Functionalizing Nanoparticles with Biological Molecules: Developing Chemistries that Facilitate Nanotechnology. *Chem. Rev.* **2013**, *113*, 1904−2074.
(51) Guardia, P.; Di Corato, R.; Lartigue, L.; Wilhelm, C.; Espinosa, A.; Garcia-Hernandez, M.; Gazeau, F.; Manna, L.; Pellegrino, T. Water-Soluble Iron Oxide Nanocubes with High Values of Specific Absorption Rate for Cancer Cell Hyperthermia Treatment. *ACS Nano* **2012**, *6*, 3080−3091.
(52) Piao, Y.; Jin, Z.; Lee, D.; Lee, H. J.; Na, H. B.; Hyeon, T.; Oh, M. K.; Kim, J.; Kim, H. S. Sensitive and high-fidelity electrochemical immunoassay using carbon nanotubes coated with enzymes and magnetic nanoparticles. *Biosens. Bioelectron.* **2011**, *26*, 3192−3199.
(53) Jun, Y. W.; Seo, J. W.; Cheon, A. Nanoscaling laws of magnetic nanoparticles and their applicabilities in biomedical sciences. *Acc. Chem. Res.* **2008**, *41*, 179−189.
(54) Sandiford, L.; Phinikaridou, A.; Protti, A.; Meszaros, L. K.; Cui, X. J.; Yan, Y.; Frodsham, G.; Williamson, P. A.; Gaddum, N.; Botnar, R. M.; Blower, P. J.; Green, M. A.; de Rosales, R. T. M. Bisphosphonate-Anchored PEGylation and Radiolabeling of Superparamagnetic Iron Oxide: Long-Circulating Nanoparticles for in Vivo Multimodal (T1MRI-SPECT) Imaging. *ACS Nano* **2013**, *7*, 500−512.
(55) Mattoussi, H.; Karasz, F. E.; Langley, K. H. Electrostatic and Screening Effects on the Dynamic Aspects of Polyelectrolyte Solutions. *J. Chem. Phys.* **1990**, *93*, 3593−3603.